A coarse-grained model for amorphous and crystalline fatty acids

K. R. Hadley[1] and C. McCabe[1,2,a)]
[1]*Department of Chemical and Biomolecular Engineering, Vanderbilt University, Nashville, Tennessee 37235-1604, USA*
[2]*Department of Chemistry, Vanderbilt University, Nashville, Tennessee 37235-1604, USA*

(Received 18 December 2009; accepted 20 February 2010; published online 1 April 2010)

Fatty acids constitute one of the main components of the lipid lamellae in the top layer of the skin, known as the stratum corneum, which acts as a barrier to foreign substances entering the body and to water leaving the body. To better understand the mechanics of the skin, a molecular-level understanding of the structure of the lamellae needs to be investigated. As a first step toward this goal, the current work involves the development of a coarse-grained model for fatty acids in an amorphous and a crystalline state. In order to retain the structural details of the atomistic molecules, radial distribution functions have been used to provide target data against which the coarse-grained force field is optimized. The optimization was achieved using the method developed by Reith, Pütz, and Müller-Plathe with a damping factor introduced into the updating scheme to facilitate the convergence against the crystalline radial distribution functions. Using this approach, a transferable force field has been developed for both crystalline and amorphous systems that can be used to describe fatty acids of different chain lengths. We are unaware of any other coarse-grained model in the literature that has been developed to study solid phases. Additionally, the amorphous force field has been shown to accurately model mixtures of different free fatty acids based on the potentials derived from pure lipid systems. © *2010 American Institute of Physics*. [doi:10.1063/1.3360146]

I. INTRODUCTION

Even though the skin is the largest organ in the body,[1] the mechanics of the skin's functions are not well understood compared with other major organs. One of the main roles of the skin is to act as a barrier to foreign agents entering, and prevent water loss from, the body. The barrier function of the skin is controlled by the outermost layer, called the stratum corneum, which consists of dead skin cells (corneocytes) embedded in a complex crystalline lipid matrix. The corneocytes are believed to be impenetrable to water and solutes and are arranged in a brick (corneocytes) and mortar (lipid lamellae) fashion, giving rise to a tortuous diffusion pathway[2] through the skin barrier. The main components of the lipid matrix are ceramides, free fatty acids, and cholesterol,[3] and have all been shown to be essential to the structure of the lipid lamellae.[4,5] A reduction in the amount of free fatty acids in the stratum corneum, in particular, can alter the lipid matrix from a orthorhombic crystal structure to a more permeable hexagonal organization,[5] which is seen in skin diseases, such as ichthyosis, that are linked to impaired barrier function.[6]

In the stratum corneum, the hydrocarbon chains of the fatty acids range from 20 to 30 carbons in length,[7] with the majority having an even number of carbons and C24:0 (tetracosanoic acid, also known as lignoceric acid) and C26:0 (hexacosanoic acid) being found in the highest mol %. Here the notation C24:0 refers to an acid with 24 carbons and 0 degrees of unsaturation. While it is known that a deficiency of free fatty acids (as opposed to fatty acids bound to corneocytes) in the stratum corneum causes a structural phase change,[5] little is known about the molecular level interactions causing the observed behavior. By performing molecular simulations of the lipids of the stratum corneum, we hope to gain insight into how and why a phase change occurs. Such simulations would naturally involve a complex lipid mixture and therefore require the study of temporal and spatial scales likely beyond the capability of atomistic simulations; although atomistic simulations can provide a wealth of information at the molecular level, they are limited to short length and time scales making self-assembly in mixed lipid systems, which can occur on the nano- to microsecond time scale, difficult to probe via atomistic simulation.[8–11] We are therefore focusing on the development of coarse-grained models, in which a degree of the atomistic detail is sacrificed, and larger length and time scales can be more easily studied.

Coarse-grained models have been widely used in studies of biological membranes and are based primarily on the phospholipid dipalmitoylphosphatidylcholine (DPPC). Several coarse-grained models have been developed in the literature to observe self-assembly, membrane dynamics, structural properties, and phase behavior, all using a myriad of different techniques.[8–11] While each technique is different in the details of the approach, they all share common underlying principles, namely, to reduce the number of accountable sites compared with the atomistic model and to optimize the behavior of the model to match target properties, while sacrificing inconsequential attributes or information. The atomistic level information and properties against which the model is to be optimized are initially determined based on

a)Author to whom correspondence should be addressed. Electronic mail: c.mccabe@vanderbilt.edu.

the properties thought to control the target behavior; however, if during the model development the target features cannot be reproduced, the information considered may be revisited to include an important attribute that was initially sacrificed. For an overview of the development and application of coarse-grained models the reader is directed to recent reviews.[11,12]

While coarse-grained models have to date been successful in modeling liquidlike membranes (see, for example, Refs. 9 and 10), polymers (see, for example, Refs. 13 and 14), liquid crystalline,[15] and glassy states,[16] we are unaware of any previous work on developing a coarse-grained model for a solid crystalline state. Rather than develop a completely new force field for fatty acids we initially investigated the possibility of using a coarse-grained force field, such as the Martini force field, from the literature; however, we were unable to reproduce crystal structures. The problems with solid phases within the Martini force field were recently noted by Marrink and co-workers.[17]

The remainder of the paper is organized as follows. The overall strategy used to develop a coarse-grained force field for fatty acids is first described. The simulation details are then discussed followed by an overview of how the chosen coarse-graining method was used. Given the semicrystalline nature of the fatty acids in the stratum corneum, results are presented for simulations performed both in amorphous and crystalline states.

II. COARSE-GRAINED MODEL

When developing a coarse-grained model it is essential to identify the target properties that the model should duplicate and the behavior of the target system that can be considered inconsequential to the model's goal. Since the key impact of the fatty acids on the stratum corneum is structural,[5] our goal was to develop a coarse-grained force field capable of mimicking these effects. Due to the scarcity of experimental structural measurements for fatty acids, the necessary target data for the coarse-grained force field optimization were radial distribution functions (RDFs) taken from atomistic simulations of the fatty acids. Therefore, in order to ensure accurate results on the coarse-grained level, the atomistic model must accurately reflect the experimental behavior.

The CHARMM force field[18] was chosen to describe the fatty acids at the atomistic level due to its success in modeling similar biological systems. Although there are no experimental data available in the literature for fatty acids in an amorphous state, limited experimental data are available for fatty acids in the crystalline state against which the atomistic force field can be validated. In particular, melting point data have been reported for C16:0, C24:0, and C26:0, and the crystal structure for C16:0 has been determined by Moreno *et al.*[19] Additionally, Moreno hypothesizes that the C16:0 data can be extrapolated to acids of longer chain lengths. Molecular dynamics simulations of C16:0, C24:0, and C26:0 have, therefore, been performed for validation purposes and simulations of C24:0 and C26:0 were subsequently chosen as the basis for the coarse-grained model development, since C24:0 and C26:0 are the predominant fatty acids in the stratum corneum.[7]

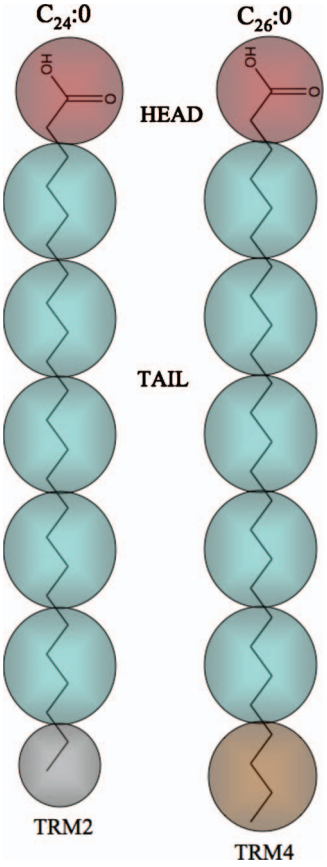

FIG. 1. Schematic illustrating the mapping of C24:0 and C26:0 fatty acids to the coarse-grained level.

In Fig. 1, we present the mapping of the C24:0 and C26:0 fatty acids to the coarse-grained level. In order to simplify the development of an accurate fatty acid coarse-grained force field, the mapping was designed to use the minimum number of bead types possible, in order to minimize the number of interactions that needs to be optimized, and enable the potentials to be transferable to molecules for which they were not optimized. As shown in Fig. 1, the acid head group represents one bead (denoted HEAD), while every four subsequent carbons are described by tail bead (denoted TAIL). The two terminal beads (denoted TRM2 or TRM4) correspond to the last two or last four carbons in the hydrocarbon tail, respectively. This mapping was chosen for its simplicity and transferability. In this work, C26:0 was chosen as the basis for determining the intermolecular interactions for the coarse-grained potential. The optimized shared interactions (HEAD-HEAD, HEAD-TAIL, and TAIL-TAIL) were then used in simulations of the coarse-grained C24:0 model, while optimizing the missing nonbonded interactions (i.e., HEAD-TRM2, TAIL-TRM2, and TRM2-TRM2). In this way, an accurate transferable coarse-grained potential for pure fatty acids can be developed.

III. SIMULATION DETAILS

All simulations were performed using the molecular dynamics package DL_POLY (version 2.14) in the isothermal-

TABLE I. Comparison of crystallographic data for C16:0 from experiment (Ref. 19) and atomistic molecular dynamics simulations.

	Expt.[a]	Simulation	
Volume (Å^3)	1658	1630	±9
a (Å)	35.62	39.07	±0.230
b (Å)	4.949	4.568	±0.023
c (Å)	9.406	9.160	±0.053
α	90.00°	91.64°	±0.577
β	90.00°	87.51°	±0.314
γ	90.45°	87.44°	±0.479
ρ (g/cm^3)	1.027	1.044	±0.006

[a]Reference 19.

isochoric (NVT) and constant stress ($N\sigma T$) ensembles with a 1 fs time step and the Nosé–Hoover thermostat and barostat for temperature and pressure control as needed.[20,21]

For the atomistic simulations of crystalline fatty acids, the molecules were initially arranged according to the crystal structure provided by Moreno *et al.*[19] For C16:0, 96 molecules were placed on a crystal lattice and the system equilibrated for 350 ps. For the larger acids studied, 160 molecules were used. The simulations were performed at 298 K and 1.0 bar in the $N\sigma T$ ensemble, which allows the shape and size of the simulation cell to change, if appropriate, from the initial configuration to a more stable crystalline structure. All simulations were run for 1.0 ns and the system density and crystal parameters determined. From a comparison to data from a 5 ns simulation for C16:0, the RDFs were found not to change significantly and so 1 ns was determined to be sufficient for subsequent simulations. To evaluate the melting point of the acids, simulations were performed using the same initial conditions at a series of different temperatures around the experimental melting point, and the density and self-diffusion coefficient were determined to be used as signatures for the melting transition.

Although fatty acids found in the skin are predominately in a crystalline state, there are no experimental data for crystalline mixtures. Therefore, simulations in the amorphous state must be used to collect radial distribution function data for parametrization of the cross interactions in the coarse-grained model. For each amorphous simulation, 100 molecules were placed on an orthorhombic lattice and equilibrated for 1 ns, at which point the system contained no apparent defined structure. Production runs in the NVT and isothermal-isobaric (NPT) ensemble were then performed for an additional 1.0 ns at 298 K and 1.0 bar. The mapping in Fig. 1 was subsequently applied to the resulting atomistic trajectories based on the center of mass of the atoms in each bead to obtain the target RDF data on the coarse-grained level.

In simulations with the coarse-grained model, in both the amorphous and crystalline states, the same simulation conditions and initial configurations were used as for the counterpart atomistic simulations. The coarse-grained potential optimization was performed using the iterative Boltzmann inversion method of Reith, Pütz, and Müller-Plathe (RPM). To our knowledge, the RPM method has to date only been applied to liquids and liquid crystalline or amorphous solid

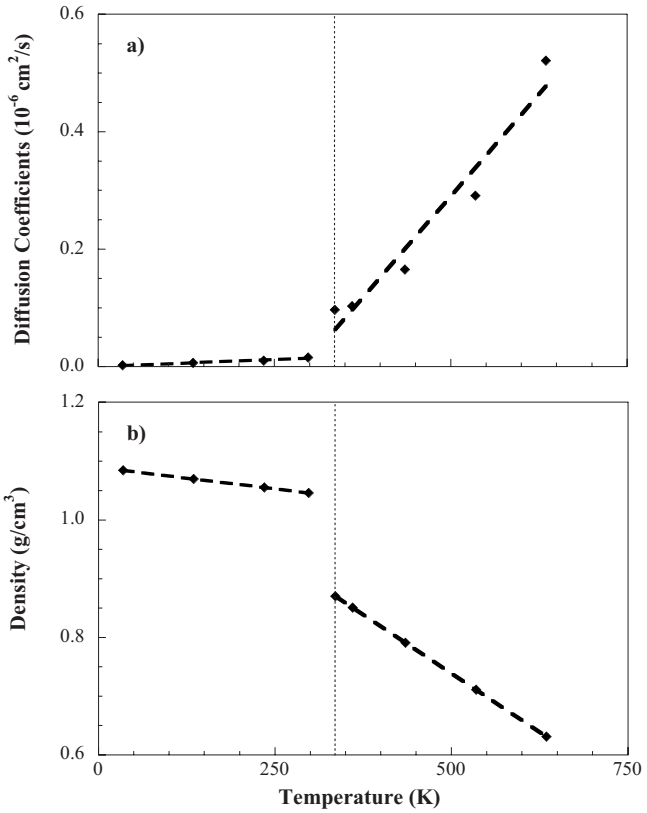

FIG. 2. (a) Diffusion coefficients and (b) density for C16:0 as a function of temperature from atomistic molecular dynamics simulations (diamonds). The dashed lines are provided as a guide and the experimental melting point is indicated by the dotted line.

systems.[13–15,22,23] The crystal potential optimization was performed in an $N\sigma T$ ensemble, therefore the pressure correction process in the original RPM method was not implemented. In addition, in the amorphous state, we found that the pressure correction was ineffective in matching the atomistic pressure and RDF simultaneously. To ensure the amorphous system had an appropriate pressure, the potential was optimized in the NPT ensemble and then reoptimized in the NVT ensemble with the NPT optimization as a new starting point. After the NPT optimization and an NVT reoptimization, the coarse-grained system at an elevated pressure had a comparable density to that observed in the atomistic simulation.

IV. METHODOLOGY

Within the RPM method both the intermolecular and intramolecular components of the coarse-grained force field are based on the target atomistic trajectory mapped to the coarse-grained level; the intermolecular interactions (electrostatic and van der Waals interactions which are consolidated into one numerical potential) are optimized iteratively against the target atomistic data while the intramolecular interactions (bond stretching, bond bending, and torsional motion between coarse-grained sites) are calculated explicitly from the target atomistic data. Below we briefly describe the parametrization process as implemented in this work.

The parameters for the bond stretching and angle forces are based on a Gaussian-based potential derived from a his-

TABLE II. Comparison of crystallographic data for C26:0 from atomistic and coarse-grained simulations and experimental data (Ref. 19) extrapolated from the C16:0 crystal structure.

	Estimated Expt.	Atomistic		Coarse-grained	
Volume (Å^3)	2634	2618	±7	2592	±121
a (Å)	56.59	56.65	±0.18	60.07	±3.26
b (Å)	4.949	4.864	±0.017	4.869	±0.316
c (Å)	9.406	9.517	±0.023	9.062	±0.157
α	90.00°	91.37°	±0.43	88.52°	±0.29
β	90.00°	91.17°	±0.57	89.10°	±0.26
γ	90.45°	87.87°	±0.38	81.76°	±0.37
ρ (g/cm^3)	1.000	1.007	±0.003	1.017	±0.049

togram of the distance between two bonded sites (or the angle between three bonded sites) measured from the target atomistic trajectory. Before normalization, the angle distributions are weighted by a factor of $\sin(\theta)$, as given in Eq. (1),[14]

$$P(\theta) = f_n p(\theta)/\sin(\theta), \tag{1}$$

where f_n is the normalization factor, $p(\theta)$ is the distribution, $P(\theta)$ represents the normalized distribution, and θ is the angle.[14] A Gaussian was then fitted to the normalized distribution and the intramolecular potential was obtained through a Boltzmann inversion. The force constant for a harmonic oscillator and the equilibrium distance/angle emerge from the simplification of the inversion as follows:[14]

$$P(\theta) = \frac{A}{w\sqrt{\pi/2}} \exp^{-2(\theta - \theta_{\mathrm{eq}})^2/w^2}, \tag{2}$$

$$V(\theta) = -kT \ln\left(\frac{A}{w\sqrt{\pi/2}} \exp^{-2(\theta - \theta_{\mathrm{eq}})^2/w^2}\right), \tag{3}$$

$$V(\theta) = \frac{2kT}{w^2}(\theta - \theta_{\mathrm{eq}})^2 + \mathrm{const}, \tag{4}$$

where A is the Gaussian area, w the Gaussian width, θ_{eq} the equilibrium angle, k the Boltzmann constant, and T the temperature. Unlike the original RPM method, the coarse-grained force field developed here also includes a torsional potential between each four consecutive sites to aid the coarse-grained molecules in retaining their structure. Since dihedral potentials are typically oscillatory and do not follow a Gaussian distribution, the same parameters as in the atomistic CHARMM force field for rotation along the carbon-carbon bond were used for the dihedral in the coarse-grained model.

In the RPM method, the nonbonded potential is obtained from an iterative optimization to fit the coarse-grained RDFs to those obtained from the atomistic target trajectory mapped to the coarse-grained level. In all cases either a Lennard-Jones potential or a previously optimized potential for a similar interaction was used as the initial guess for the nonbonded interactions, and the RDFs were calculated and the potentials updated via a Boltzmann inversion,

$$V_{j+1}(r) = V_j(r) + kT \ln\frac{g_j(r)}{g^*(r)}, \tag{5}$$

where $V_j(r)$ is the potential, $g_j(r)$ is the coarse-grained RDF, and $g^*(r)$ is the target RDF at distance r and iteration number j. For the crystalline system, we found that the optimization of the potential was ill defined due to the fact that the resultant RDF for each subsequent iteration had a diverging oscillatory response that resulted in large changes in the potential and caused the cell volume to either contract to a size too small for the defined cutoff or expand to a gaseous state. This behavior likely stems from the high order of repetition in a crystalline state, leading to sharp, tall peaks with low valleys in the RDFs in contrast to a liquid or amorphous state, where a large degree of sampling with respect to orientation leads to broad, short peaks. To overcome this problem, Eq. (5) was modified to include a damping factor[23] δ, viz.,

$$V_{j+1}(r) = V_j(r) + \delta kT \ln\frac{g_j(r)}{g_*(r)}. \tag{6}$$

Throughout the optimization, the magnitude of δ correlates with the stability of the optimization and was always less than 1.0 and never negative. In amorphous optimizations, the damping factor was not needed, therefore a value of 1.0 was used in Eq. (6).

V. RESULTS AND DISCUSSION

A. Atomistic force field validation

In order to ensure that the atomistic simulations generate an appropriate target trajectory for the coarse-graining procedure, the atomistic force field was first validated against experimental data. For validation purposes, we focused on C16:0 as both experimental crystal structure and melting point data are available for hexadecanoic acid.[19] From Table I, in which we compare the experimental crystal unit cell parameters and density with those obtained from the atomistic simulations, we can see that the predicted crystal parameters are in good overall agreement with the experimental values. The density and the unit cell angles are within 2% and 3% of the experimental data, respectively, while the a vector is within 3% and the b and c vectors deviate by 10% and 8%, respectively. Fatty acids can exhibit multiple crystal structures at room temperature, which may account for the small discrepancies observed.[19]

TABLE III. Comparison of crystallographic data for C24:0 from atomistic and coarse-grained simulations and experimental data (Ref. 19) extrapolated from the C16:0 crystal structure.

	Estimated Expt.	Atomistic		Coarse-grained	
Volume (Å^3)	2439	2445	±8	2345	±84
a (Å)	52.40	52.79	±0.18	55.93	±1.88
b (Å)	4.949	4.874	±0.015	4.647	±0.282
c (Å)	9.406	9.517	±0.036	9.087	±0.168
α	90.00°	88.84°	±0.54	90.41°	±1.27
β	90.00°	89.69°	±0.28	89.69°	±1.45
γ	90.45°	87.26°	±0.73	88.15°	±6.86
ρ (g/cm^3)	1.004	1.002	±0.003	1.044	±0.033

In Fig. 2(a), we present the self-diffusion coefficient for C16:0 measured as a function of temperature from atomistic simulations around the experimental melting point. As can be seen from the figure, the diffusion coefficients at low temperatures are small and exhibit little change with temperature, as is typical for a system in the solid state; however, once the temperature approaches values close to the experimental melting point, the diffusion coefficient is seen to increase significantly and a distinctive change in the slope of the diffusion coefficient as a function of temperature is observed, indicating the onset of a phase change to the liquid state. We note that a similar trend is observed for the system density as a function of temperature [shown in Fig. 2(b)], in that at the melting point there is a discontinuity in the density indicating that the system has undergone a phase change from solid to liquid state.

Although no experimental data are available for the crystal structure of C24:0 and C26:0, as discussed earlier, we can compare the predicted crystal structures with those extrapolated from the data of Moreno *et al.*[19] The results presented in Tables II and III for C26:0 and C24:0, respectively, exhibit similar trends compared with C16:0 with respect to the deviations in the simulation results compared with the estimated experimental parameters. Specifically, for both acids, the predicted density and unit cell parameters are within 2% of the values extrapolated from the crystal structure of C16:0, with the exception of the γ angle for which the deviation is 2.9% for C26:0 and 3.5% for C24:0. The predicted melting point transitions are again found to be in good agreement with the experimental data as measured by the change in the diffusion coefficient (Fig. 3) and density (not shown), again indicating that the atomistic system is capturing the fatty acid phase behavior. Although these observations are indirect measures of the melting point, they indicate that the CHARMM force field can capture the phase change behavior of the fatty acids and therefore the force field can be used to generate the target data on which to base the coarse-grained model.

B. Coarse-grained bonded potential

For parametrization of the coarse-grained bonded potential, bond length and bond angle distributions mapped to the coarse-grained level were extracted from both the atomistic amorphous and crystal simulations. To match the functional form of the CHARMM force field as described above, the bond length distributions were then fitted to single peak Gaussian distributions. For illustrative purposes, in Fig. 4, we show the bond length distribution and the corresponding Gaussian fit for two TAIL beads from a crystal simulation of C26:0.

From the amorphous simulations, we found that the bond distributions compared well with those obtained from simulations of a single molecule *in vacuo*; the latter approach being used by Peter and co-workers[15] with the RPM method to parametrize a coarse-grained model for azobenzene liquid crystals. The bond parameters were, therefore, arbitrarily taken from the amorphous simulations. For the bond angles, using the amorphous simulation data or the single molecule calculations, no definitive distribution is observed on the coarse-grained level. In both cases, the angles of the target coarse-grained molecule essentially have an equal probability of being measured at any value. Since it is therefore not possible to apply the RPM method to determine the angle parameters, those for the hydrocarbon tails in the coarse-grained MARTINI force field[10] for DPPC were used. The DPPC hydrocarbon tails are structurally identical to those found in the fatty acids studied in this work and the DPPC MARTINI force field has been successfully used to study lipid bilayer systems.[10,17]

From the crystal simulations, if we compare the bond-length distributions to those obtained from a single molecule *in vacuo*, the location of the Gaussian peak was found to be

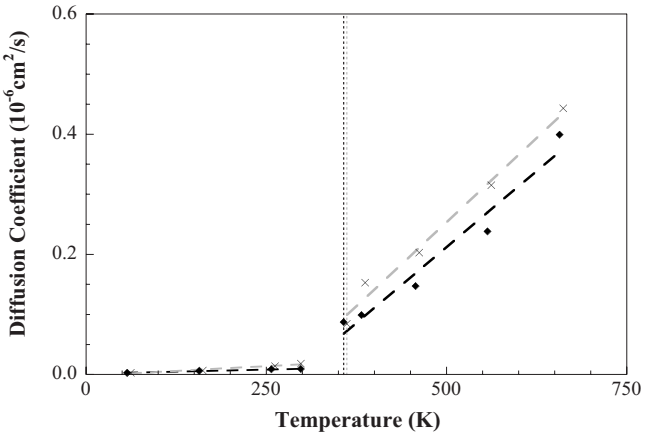

FIG. 3. Diffusion coefficients for C24:0 (diamonds, black lines) and C26:0 (crosses, gray lines) as a function of temperature from atomistic molecular dynamics simulations. The dashed lines are provided as a guide and the experimental melting point is indicated by the dotted line.

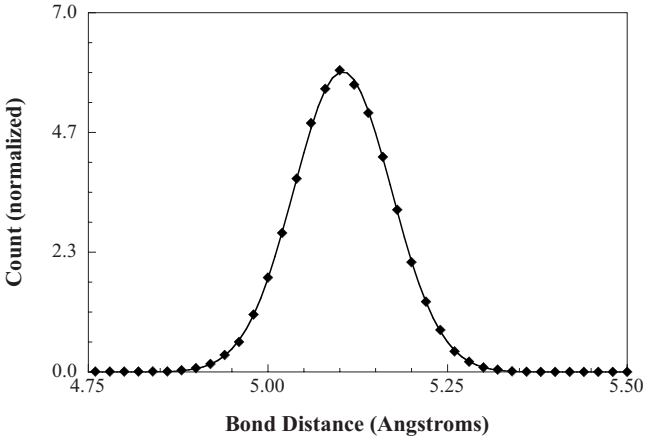

FIG. 4. Probability distribution for a TAIL-TAIL bond length from an atomistic trajectory (diamonds) and fitted by a Gaussian curve (solid line).

at larger distances and the width of the peak much smaller, resulting in higher force constants. As such, the bonds are tighter and longer in the crystal than in the amorphous state (or measured from a single molecule *in vacuo*). For the angles, in contrast to the amorphous state, the angle distributions could be determined from the atomistic crystal simulation and were found to be very similar to those used in the MARTINI force field, with the force constants being slightly higher in the crystal. In initial simulations of crystalline fatty acids with the coarse-grained model, the intramolecular force field parameters from the amorphous state simulations were used, as it was considered that the potentials derived from the crystal could make the coarse-grained molecules too stiff and inhibit the ability of the molecules to move around each other; however, model convergence issues were discovered that were alleviated if the longer bond lengths taken from the crystal simulations were used. Therefore, it was concluded that in order to match the target RDF and produce accurate crystal structures from the coarse-grained model, the longer bonds seen in the crystal system need to be retained but the flexibility of the looser bonds from the amorphous simulations can be used. All of the bonded parameters used in this work are reported in Table IV.

C. Nonbonded potential optimization

1. The amorphous state

The numerical potentials for all bead interactions in C26:0 (i.e., HEAD-HEAD, TAIL-TAIL, TRM4-TRM4, HEAD-TAIL, HEAD-TRM4, and TAIL-TRM4) were optimized to enable the coarse-grained RDFs to match the target atomistic RDFs mapped to the coarse-grained level, indicating structural agreement between the atomistic and coarse-grained simulations. Representative radial distribution functions are shown in Fig. 5 for the TAIL-TAIL, HEAD-HEAD, HEAD-TAIL, and TRM4-TRM4 interactions from a C26:0 amorphous simulation. To avoid repetition, the other RDFs are not shown as they all exhibit the same general trends and level of agreement between the coarse-grained and target RDF. The transferability of the coarse-grained potentials was then tested by using the HEAD-HEAD, HEAD-TAIL, and TAIL-TAIL interactions parametrized for C26:0 in coarse-grained simulations of C24:0 while optimizing the new interactions (i.e., HEAD-TRM2, TAIL-TRM2, and TRM2-TRM2). The results of the optimized interactions are not shown as the agreement obtained is comparable to that seen in C26:0; however, the RDFs of the transferred interactions are presented in Fig. 6 for the TAIL-TAIL, HEAD-HEAD, and HEAD-TAIL interactions to illustrate the retained agreement with their atomistic counterpart and transferability of the potentials developed.

As an additional test of the transferability of the amorphous fatty acid coarse-grained force field, a mixed lipid system in an amorphous arrangement has been studied. The missing TRM2-TRM4 cross bead interaction needed to study mixed lipid systems was first optimized from a simulation of an equimolar mixture of C24:0 and C26:0, and a good agreement between the target and fitted RDF was obtained. A more complex atomistic amorphous mixture of the stratum corneum fatty acids in the molar composition reported by Norlén *et al.*[7] (listed in Table V) was then studied. The atomistic simulation was run from a random amorphous configuration and RDF data were collected to provide the target for comparison to the results from the coarse-grained force field. To reiterate the information from Sec. III, this amorphous state was established by equilibrating over 300 ps at

TABLE IV. Coarse-grained model bonded potential parameters for amorphous and crystalline fatty acids.

Bond	Force constant (kcal/mol/Å^2)	Amorphous equilibrium distance (Å)	Crystal equilibrium distance (Å)
HEAD-TAIL	12.022	3.8998	4.1229
TAIL-TAIL	6.205	3.9834	5.0902
TAIL-TRM4	7.111	3.9748	4.7917
TAIL-TRM2	6.01	3.1614	3.8790
Angle	**Force constant (kcal/mol)**	**Amorphous equilibrium angle**	**Crystal equilibrium angle**
HEAD-TAIL-TAIL	0.018	180.0	180.0
TAIL-TAIL-TAIL	0.018	180.0	180.0
TAIL-TAIL-TRM4	0.018	180.0	180.0
TAIL-TAIL-TRM2	0.018	180.0	180.0

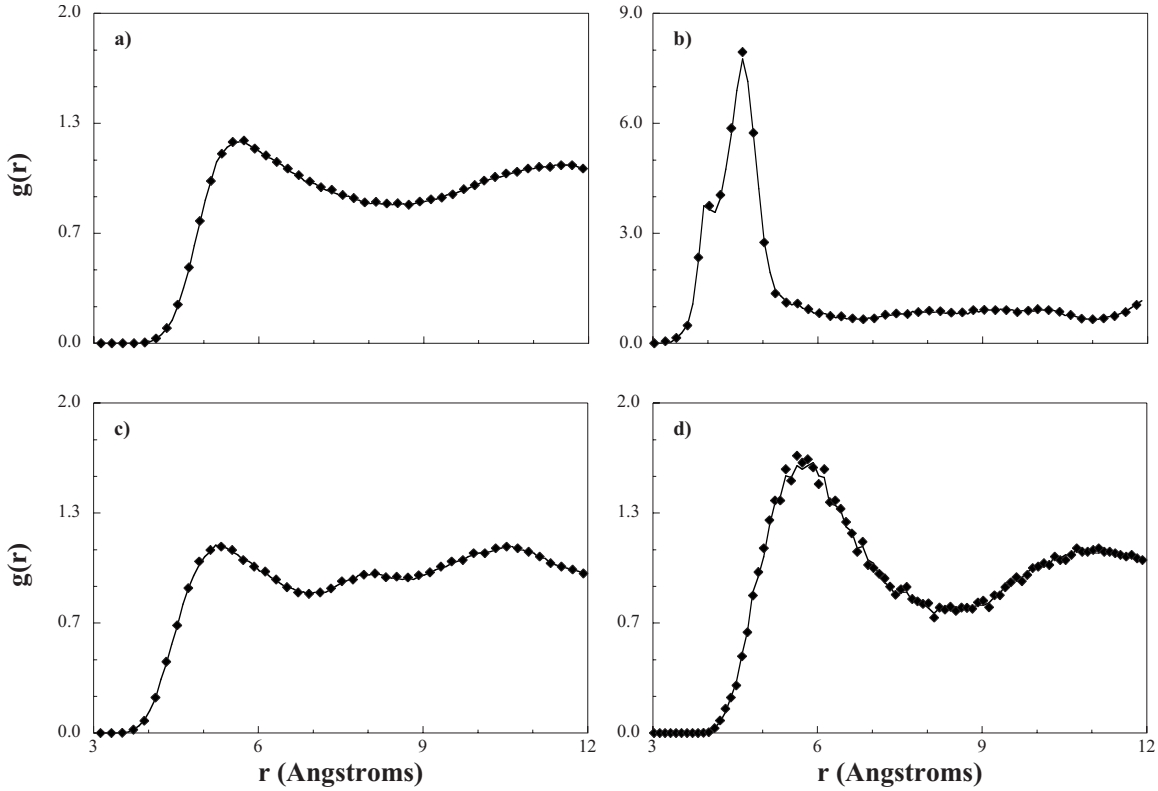

FIG. 5. Radial distribution function between (a) tail (TAIL-TAIL), (b) head (HEAD-HEAD), (c) tail and head (TAIL-HEAD), and (d) terminal (TRM4-TRM4) beads in C26:0 from a coarse-grained amorphous simulation (diamonds) and from the target amorphous atomistic simulation (solid line).

an elevated temperature to allow for a well mixed state among the different fatty acids. Since terminal beads for odd numbered acids are not considered in our coarse-grained force field due to the relatively low mol % of odd-numbered acids in the stratum corneum, the odd-numbered acids were described as even-numbered ones in the coarse-grained system, i.e., one half of the C25:0 molecules were modeled as C24:0 and the other half modeled as C26:0. A comparison of the target RDFs and the coarse-grained model prediction is shown in Fig. 7 for the HEAD-HEAD, TAIL-TAIL, HEAD-TAIL, and TRM4-TRM4 interactions. Similar to the behavior seen in Fig. 6 when using transferred potentials from C26:0 to study C24:0, a very good agreement is obtained in the mixed lipid system, further supporting the accuracy and transferability of the coarse-grained models developed. By comparing Fig. 7 with Figs. 5 and 6, we can also see that the structuring of the beads in this complex mixture on the atomistic level is very similar to the structure of the acids in pure systems. Therefore, we can assess that the results from the mixture are as accurate as those found in the pure state.

2. The crystalline state

As discussed earlier, the higher order of structure seen in the crystal compared with the amorphous simulations caused the optimization to be ill defined and required the introduction of a damping factor into Eq. (5) to enable the convergence to be achieved. We also found that in general the optimization of the crystalline potentials requires more iterations than in the amorphous state. To illustrate the need for the damping factor in Eq. (6), RDFs from iterations of the TAIL-TAIL potential for C26:0 with and without the use of the damping factor are shown in Fig. 8(a). From the figure we can see that the RDF has multiple sharp peaks, as expected for a solid state, and that without the damping factor the coarse-grained RDF is found to alternate between states A and B in the optimization, with the magnitudes of the peaks becoming larger instead of converging toward the target. By making the changes in the potential smaller between iterations through the use of the damping factor, the minimization of the difference between the coarse-grained RDF and the target RDF can occur and the resultant potential allows for the coarse-grained RDF to match its target (state C). Although the optimized structure (state C) produces higher peaks and lower valleys than the target, the position of the peaks and valleys is retained. A similar agreement is obtained for the other pure coarse-grained interactions (i.e., HEAD-HEAD, HEAD-TAIL, and TRM4-TRM4), as shown in Figs. 8(b)–8(d), again indicating that the coarse-grained crystal has the same structure as seen in the atomistic simulations. This can be further confirmed by comparing the crystal parameters from the coarse-grained simulation with those obtained from the atomistic simulation and the extrapolated experimental values in Table II. The coarse-grained crystal parameters, reported in Table II, are found to be in good agreement with their atomistic counterparts, with only two parameters (the γ angle and the length of the a vector) having a percent difference greater than 5%. The small discrepancy between the RDF of the coarse-grained system and the target may account for the observed deviations. We note that although the system is in a solid state and so molecular mo-

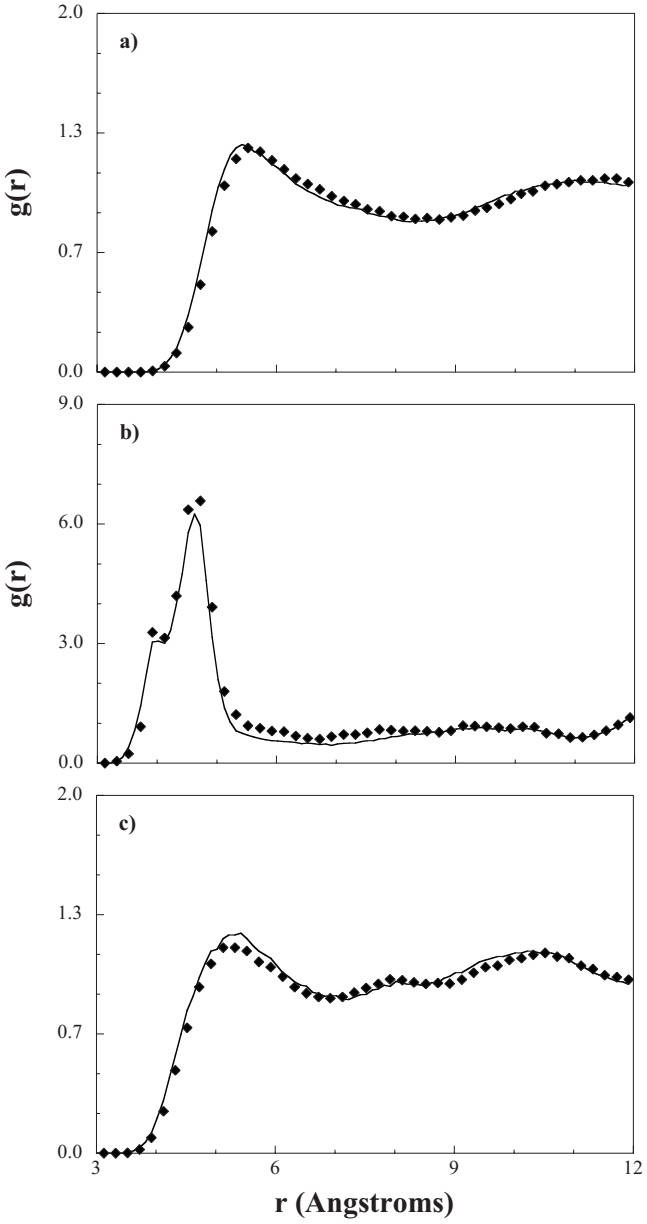

FIG. 6. Radial distribution function between (a) tail (TAIL-TAIL), (b) head (HEAD-HEAD), and (c) tail and head (TAIL-HEAD) beads in C24:0 from a coarse-grained amorphous simulation (diamonds) and the target atomistic simulation (solid line). The coarse-grained potential for the interactions is transferred from C26:0.

tion is limited, changes in crystal structure were observed during the iterative process, indicating that the final crystal structure from the coarse-grained model is stable. During the optimization procedure significant deviations were in some cases observed between the coarse-grained RDFs and the atomistic targets, indicating that the molecules moved away from the initial experimental crystal structure to a structure that was more appropriate for the potential at that iteration. The differences in crystal structure could also be confirmed by visualization and comparison of configurations from the coarse-grained and atomistic simulations.

As in the amorphous simulations, the HEAD-HEAD, TAIL-TAIL, and HEAD-TAIL crystal potentials of C26:0 were then transferred and used in a crystalline C24:0 simulation in which the missing interactions (HEAD-TRM2, TAIL-TRM2, and TRM2-TRM2) were then optimized. The optimized potentials were found to be in good agreement with the target data and the transferred potentials performed well for C24:0, as shown in Fig. 9, for the TAIL-TAIL, HEAD-HEAD, and HEAD-TAIL RDFs. While the peaks in the RDF shown in Fig. 9 are higher in the coarse-grained simulation compared with the atomistic target, they are in the correct positions. This would indicate that the "size" of the coarse-grained beads is appropriate, but the interactions could be too strong, promoting a higher degree of structure than is seen in the atomistic simulation. This could also be due to the use of the force constants from the amorphous state (which were weaker than those derived from the crystal simulations), for which the nonbonded interactions need to be stronger to promote the retention of the crystal symmetry and structure. As seen in Table III, the predicted crystal structure for C24:0 is, however, still in good agreement with the pseudoexperimental data and the atomistic system; the only two values with a greater than 5% difference than the extrapolated values are the *b* and *c* vectors.

Finally a snapshot from the simulation of C24:0 at both the atomistic and coarse-grained levels is shown in Fig. 10. From the figure, and confirmed by the agreement in the RDFs, we can see that the structures are in good agreement. Specifically, the hydrogen-bonding network is contained within the same cross-sectional plane as in the atomistic crystal and the angle between the plane and the acid tails of $37.28° \pm 2.76°$ in the atomistic simulations is reproduced on the coarse-grained level ($36.97° \pm 3.51°$). The retention of the hydrogen-bonding network can also be verified by comparing the average distance between hydrogen-bonded HEAD beads in both simulations, as depicted in Fig. 11. The average distance from the target trajectory is 5.563 Å with a standard deviation of 0.785, while the average distance from the coarse-grained simulation is 5.113 Å with a standard deviation of 0.429. Finally, the retention of the spacing of the molecules in the coarse grained model compared with the atomistic simulation can be visually verified from the snapshot shown in Fig. 10.

VI. CONCLUSIONS

Accurate and robust coarse-grained force fields have been developed for fatty acids in both the crystalline and the amorphous states at room temperature and pressure (298 K and 1 bar). When developing a coarse-grained force field,

TABLE V. Composition of free fatty acids seen in the stratum corneum (Ref. 7) and used in this work in the simulation of a mixed lipid system.

Acid	C20:0	C22:0	C24:0	C25:0	C26:0	C27:0	C28:0	C29:0	C30:0
Median mol %	4	11	39	10	23	3	8	0	2

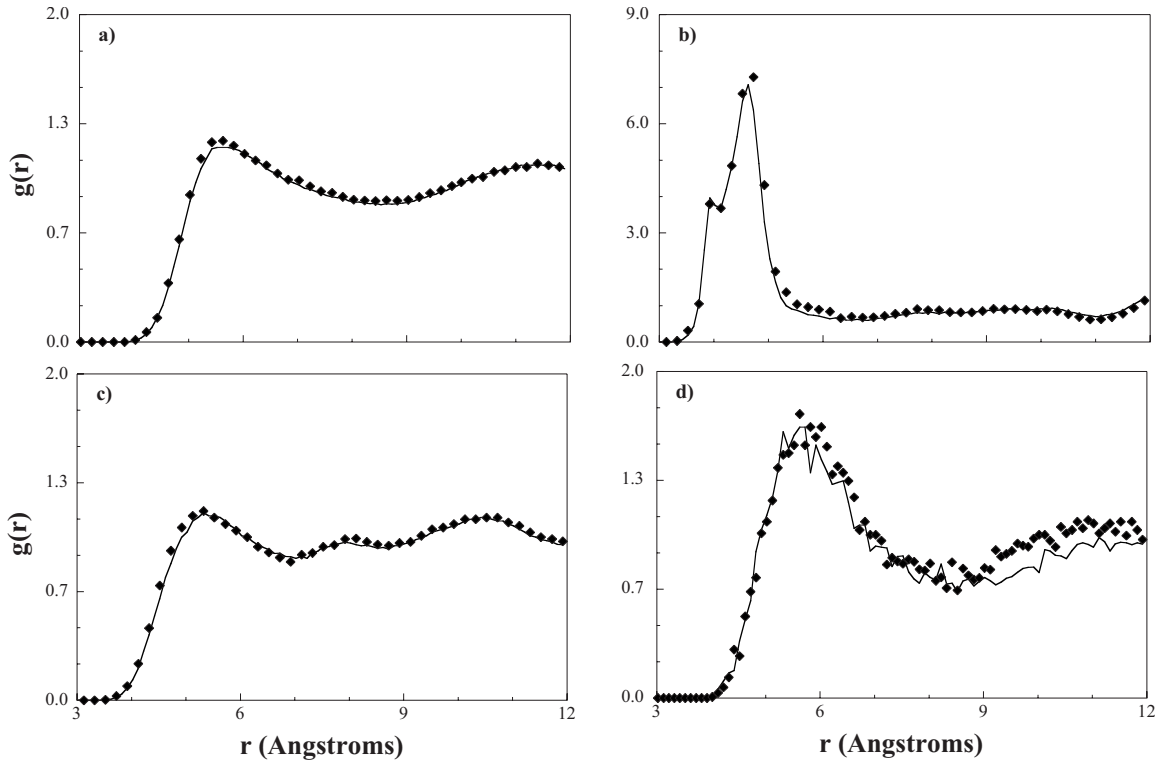

FIG. 7. Radial distribution function between (a) tail (TAIL-TAIL), (b) head (HEAD-HEAD), (c) tail and head (TAIL-HEAD), and (d) terminal (TRM4-TRM4) beads from a coarse-grained amorphous simulation (diamonds) and from the target amorphous atomistic simulation (solid line) for a mixed fatty acid system.

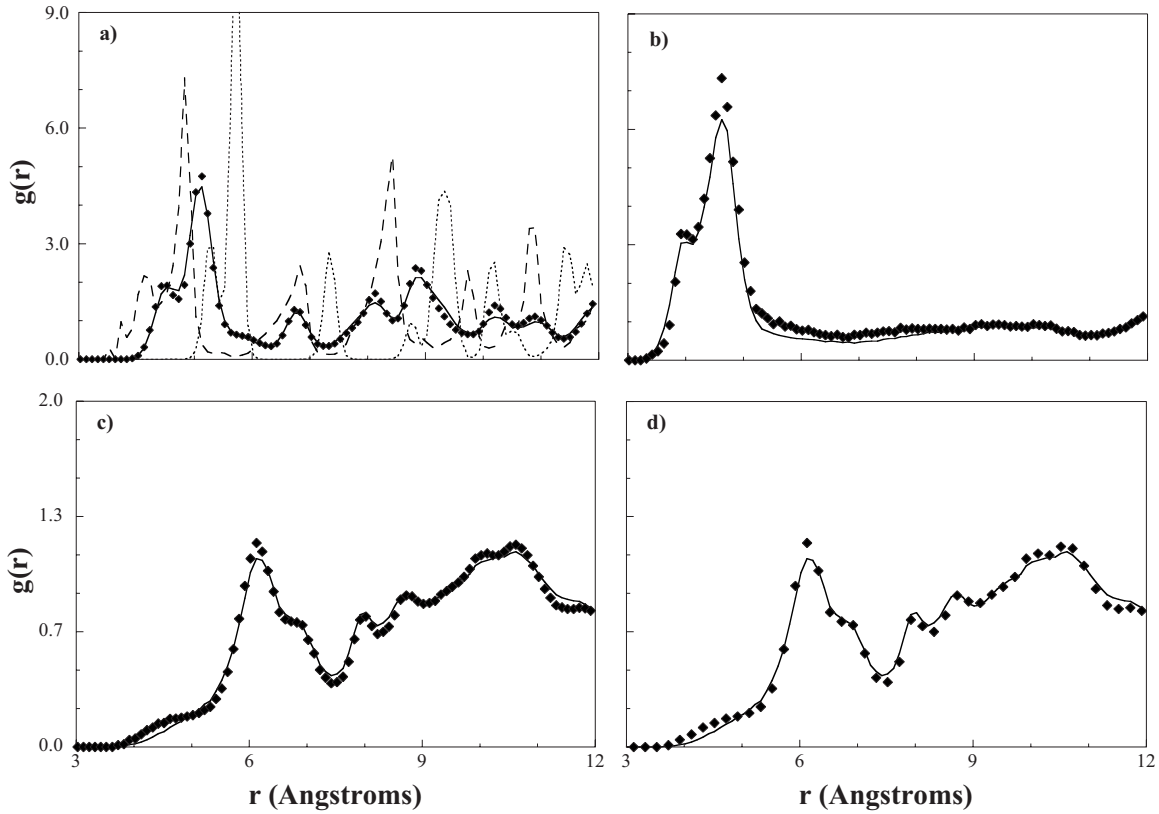

FIG. 8. Radial distribution function between (a) tail (TAIL-TAIL), (b) head (HEAD-HEAD), (c) tail and head (TAIL-HEAD), and (d) terminal (TRM4-TRM4) beads in C26:0 from a coarse-grained crystal simulation (diamonds) and the target atomistic simulation (solid line). In (a) state A (dotted line) and state B (dashed line) are from the optimization without the damping factor and state C (diamonds) from the optimization with the damping factor.

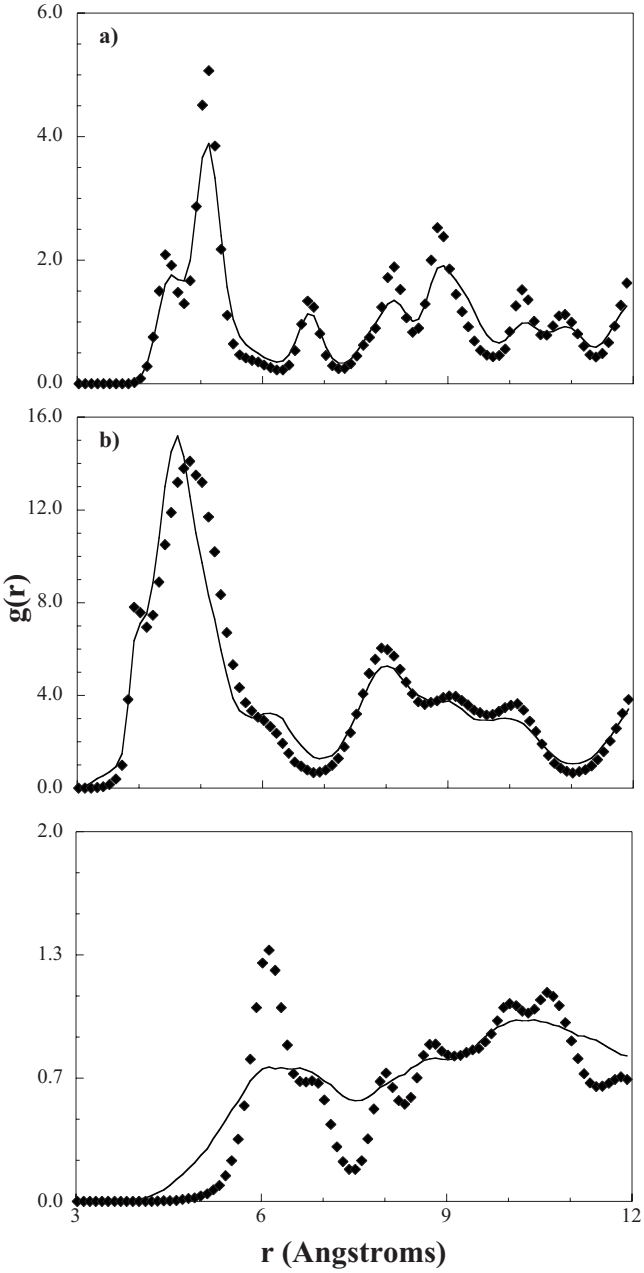

FIG. 9. Radial distribution function between (a) tail (TAIL-TAIL), (b) head (HEAD-HEAD), and (c) tail and head (TAIL-HEAD) beads in C24:0 from a coarse-grained crystal simulation (diamonds) and the target atomistic simulation (solid line). The coarse-grained potential for the interactions is transferred from C26:0.

one must decide which observable properties are to be retained on the coarse-grained level, while eliminating unnecessary atomistic details. Since we are ultimately interested in studying the structure of the fatty acids in the stratum corneum, atomistic radial distribution functions were chosen as the target property and the coarse-grained methodology developed by Reith, Pütz, and Müller-Plathe used to parameterize the model. The ability of the CHARMM all atom force field to accurately describe the fatty acids, and therefore provide reliable target data, was also verified by reproducing crystal structure data and estimating the melting point.

By incorporating a damping factor into the optimization scheme, the RPM method was found to be able to optimize

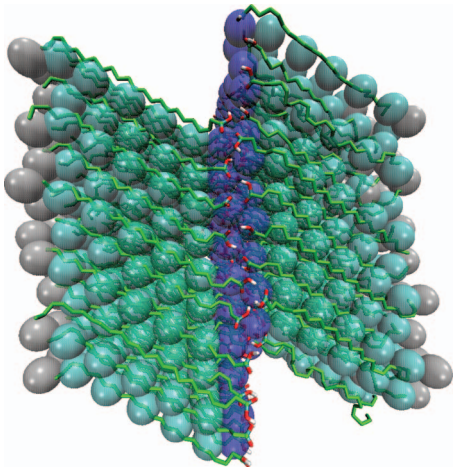

FIG. 10. Snapshot from simulations of the C24:0 crystal in the coarse-grained (transparent spheres) and atomistic (solid lines) simulations.

the coarse-grained potentials to match the RDF data from atomistic crystal simulations. The resulting crystal parameters were found to be in good agreement with experimental data, indicating that the coarse-grained model exhibits the same structural behavior as its atomistic and experimental counterparts. This result is significant given that the development of a coarse-grained model capable of reproducing a crystalline state has, to our knowledge, not yet been reported in the literature. A good agreement between the target RDFs and coarse-grained models was also obtained for the amorphous state. The robustness of the coarse-grained force fields developed for both the amorphous and crystalline states was tested by using the optimized potentials to study other fatty acids and their mixtures in a transferable fashion. In all cases, the correct structural behavior was predicted, demonstrating the accuracy and transferability of the coarse-grained models developed. We note, however, that since the potentials were optimized against atomistic simulation data at a specific temperature and pressure, as is typical for coarse-grained models, we anticipate that the models would produce RDFs away from these conditions that could deviate from the atomistic behavior. In future work coarse-grained models of cholesterol and ceramides will be developed and the role of fatty acids in the self-assembly of mixed lipid systems will be studied, and the need for amorphous versus crystalline potentials evaluated in order to accurately model the semicrystalline nature of the bilayers found in the stratum

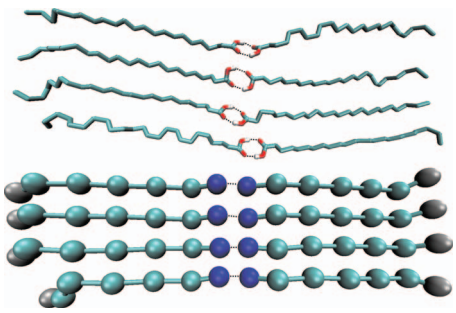

FIG. 11. Close-up of hydrogen bonding interactions (indicated by dashed lines) from atomistic (top) and coarse-grained (bottom) simulations.

corneum. Since such studies will naturally involve water, coarse-grained potentials for water and water-lipid interactions are being developed.[24]

ACKNOWLEDGMENTS

The project described was supported by the National Institute of Arthritis and Muscoskeletal and Skin Diseases (Grant No. R21 AR053270-02).

[1] *Gray's Anatomy*, edited by P. Williams (Churchill Livingstone, New York, 1995).
[2] M. S. Roberts and K. A. Watlers, in *Dermal Absorption and Toxicity Assessment*, edited by M. S. Roberts and K. A. Watlers (Marcel Dekker, New York, 1998), Vol. 91.
[3] H. J. Yardley and R. Summerly, Pharmacol. Ther. **13**, 357 (1981); P. W. Wertz, D. C. Swartzendruber, K. C. Madison, and D. T. Downing, J. Invest. Dermatol. **89**, 419 (1987); S. Law, P. W. Wertz, D. C. Swartzendruber, and C. A. Squier, Arch. Oral Biol. **40**, 1085 (1995); K. C. Madison, J. Invest. Dermatol. **121**, 231 (2003).
[4] J. A. Bouwstra, G. S. Gorris, K. Cheng, A. Weerheim, W. Bras, and M. Ponec, J. Lipid Res. **37**, 999 (1996); T. J. McIntosh, M. E. Stewart, and D. T. Downing, Biochemistry **35**, 3649 (1996); P. W. Wertz, Acta Derm Venereol **80**, 7 (2000); M. W. de Jager, G. S. Gooris, I. P. Dolbnya, W. Bras, M. Ponec, and J. A. Bouwstra, Chem. Phys. Lipids **124**, 123 (2003).
[5] J. A. Bouwstra, G. S. Gooris, F. E. R. Dubbelaar, A. M. Weerheim, A. P. Ijzerman, and M. Ponec, J. Lipid Res. **39**, 186 (1998).
[6] A. P. M. Lavrijsen, J. A. Bouwstra, G. S. Gooris, A. Weerheim, H. E. Bodde, and M. Ponec, J. Invest. Dermatol. **105**, 619 (1995).
[7] L. Norlén, I. Nicander, A. Lundsjo, T. Cronholm, and B. Forslind, Arch. Dermatol. Res. **290**, 508 (1998).
[8] R. Goetz and R. Lipowsky, J. Chem. Phys. **108**, 7397 (1998); R. Goetz, G. Gompper, and R. Lipowsky, Phys. Rev. Lett. **82**, 221 (1999).
[9] M. Kranenburg, M. Venturoli, and B. Smit, J. Phys. Chem. B **107**, 11491 (2003); T. Murtola, E. Falck, M. Patra, M. Karttunen, and I. Vattulainen, J. Chem. Phys. **121**, 9156 (2004); S. Izvekov and G. A. Voth, J. Phys. Chem. B **109**, 2469 (2005); A. P. Lyubartsev, Eur. Biophys. J. **35**, 53 (2005); S. J. Marrink, J. Risselada, and A. E. Mark, Chem. Phys. Lipids **135**, 223 (2005).
[10] S. J. Marrink, A. H. de Vries, and A. E. Mark, J. Phys. Chem. B **108**, 750 (2004).
[11] M. Venturoli, M. M. Sperotto, M. Kranenburg, and B. Smit, Phys. Rep., Phys. Lett. **437**, 1 (2006).
[12] S. Nielsen, C. Lopez, G. Srinivas, and M. Klein, J. Phys.: Condens. Matter **16**, R481 (2004); G. S. Ayton, S. Izvekov, W. G. Noid, and G. A. Voth, Curr. Top. Membr. **60**, 181 (2008).
[13] D. Reith, M. Putz, and F. Muller-Plathe, J. Comput. Chem. **24**, 1624 (2003).
[14] G. Milano, S. Goudeau, and F. Muller-Plathe, J. Polym. Sci., Part B: Polym. Phys. **43**, 871 (2005).
[15] C. Peter, L. Delle Site, and K. Kremer, Soft Matter **4**, 859 (2008).
[16] V. Molinero and W. A. Goddard, J. Phys. Chem. B **108**, 1414 (2004).
[17] S. J. Marrink, H. J. Risselada, S. Yefimov, D. P. Tieleman, and A. H. de Vries, J. Phys. Chem. B **111**, 7812 (2007).
[18] M. Schlenkric, J. Brickmann, A. D. MacKerrel, Jr., and M. Karplus, in *Biological Membranes: A Molecular Perspective from Computation and Experiment*, edited by K. M. Merz and B. Roux (Birkhauser, Boston, 1996); S. E. Feller and A. D. MacKerell, J. Phys. Chem. B **104**, 7510 (2000); S. E. Feller, K. Gawrisch, and A. D. MacKerell, J. Am. Chem. Soc. **124**, 318 (2002).
[19] E. Moreno, R. Cordobilla, T. Calvet, F. J. Lahoz, and A. I. Balana, Acta Crystallogr., Sect. C: Cryst. Struct. Commun. **62**, o129 (2006).
[20] W. Smith and T. R. Forester, J. Mol. Graphics **14**, 136 (1996); W. G. Hoover, Phys. Rev. A **31**, 1695 (1985).
[21] S. Melchionna, G. Ciccotti, and B. L. Holian, Mol. Phys. **78**, 533 (1993).
[22] H. Wang, C. Junghans, and K. Kremer, Eur. Phys. J. E **28**, 221 (2009).
[23] H. S. Ashbaugh, H. A. Patel, S. K. Kumar, and S. Garde, J. Chem. Phys. **122**, 104908 (2005); D. Bedrov, C. Ayyagari, and G. D. Smith, J. Chem. Theory Comput. **2**, 598 (2006); L. J. Chen, H. J. Qian, Z. Y. Lu, Z. S. Li, and C. C. Sun, J. Phys. Chem. B **110**, 24093 (2006); J. Elezgaray and M. Laguerre, Comput. Phys. Commun. **175**, 264 (2006); A. Rakshit and R. C. Picu, J. Chem. Phys. **125**, 164907 (2006); Q. Sun and R. Faller, Comput. Chem. Eng. **29**, 2380 (2005).
[24] K. R. Hadley and C. McCabe, "On the investigation of coarse-grained models for water: Balancing computational efficiency and the retention of structural properties," J. Phys. Chem. B (in press).